The Astrophysical Journal, 819:147 (14pp), 2016 March 10 doi:10.3847/0004-637X/819/2/147

THE ISLANDS PROJECT. I. ANDROMEDA XVI, AN EXTREMELY LOW MASS GALAXY NOT QUENCHED BY REIONIZATION*

Matteo Monelli[1,2], Clara E. Martínez-Vázquez[1,2], Edouard J. Bernard[3], Carme Gallart[1,2], Evan D. Skillman[4], Daniel R. Weisz[5,16], Andrew E. Dolphin[6], Sebastian L. Hidalgo[1,2], Andrew A. Cole[7], Nicolas F. Martin[8,9], Antonio Aparicio[1,2], Santi Cassisi[10], Michael Boylan-Kolchin[11], Lucio Mayer[12,13], Alan McConnachie[14], Kristen B. W. McQuinn[4], and Julio F. Navarro[15]
[1] Instituto de Astrofísica de Canarias, La Laguna, Tenerife, Spain; monelli@iac.es
[2] Departamento de Astrofísica, Universidad de La Laguna, Tenerife, Spain
[3] Institute for Astronomy, University of Edinburgh, Royal Observatory, Blackford Hill, Edinburgh EH9 3HJ, UK
[4] Minnesota Institute for Astrophysics, University of Minnesota, 116 Church Street, SE Minneapolis, MN, 55455 USA
[5] Astronomy Department, Box 351580, University of Washington, Seattle, WA, 98195 USA
[6] Raytheon, 1151 E. Hermans Road, Tucson, AZ 85706, USA
[7] School of Physical Sciences, University of Tasmania, Private Bag 37, Hobart 7005, TAS, Australia
[8] Observatoire astronomique de Strasbourg, Universite de Strasbourg, CNRS, UMR 7550, 11 rue de l'Universite, F-67000 Strasbourg, France
[9] Max-Planck-Institut für Astronomie, Königstuhl 17, D-69117 Heidelberg, Germany
[10] INAF-Osservatorio Astronomico di Collurania, Teramo, Italy
[11] INAF–Osservatorio Astronomico di Teramo, via M. Maggini, 64100 Teramo, Italy
[12] Department of Astronomy, The University of Texas at Austin, 2515 Speedway, Stop C1400, Austin, TX 78712, USA
[13] Department of Physics, Institut für Astronomie, ETH Zürich, Zürich, Switzerland
[14] Herzberg Astronomy and Astrophysics, National Research Council Canada, 5071 West Saanich Road, Victoria, BC V9E 2E7, Canada
[15] Department of Physics and Astronomy, University of Victoria, P.O. Box 1700, STN CSC, Victoria, BC V8W 3P6, Canada
Received 2015 June 5; accepted 2016 January 19; published 2016 March 8

ABSTRACT

Based on data aquired in 13 orbits of *Hubble Space Telescope* time, we present a detailed evolutionary history of the M31 dSph satellite Andromeda XVI, including its lifetime star formation history (SFH), the spatial distribution of its stellar populations, and the properties of its variable stars. And XVI is characterized by prolonged star formation activity from the oldest epochs until star formation was quenched ∼6 Gyr ago, and, notably, only half of the mass in stars of And XVI was in place 10 Gyr ago. And XVI appears to be a low-mass galaxy for which the early quenching by either reionization or starburst feedback seems highly unlikely, and thus it is most likely due to an environmental effect (e.g., an interaction), possibly connected to a late infall in the densest regions of the Local Group. Studying the SFH as a function of galactocentric radius, we detect a mild gradient in the SFH: the star formation activity between 6 and 8 Gyr ago is significantly stronger in the central regions than in the external regions, although the quenching age appears to be the same, within 1 Gyr. We also report the discovery of nine RR Lyrae (RRL) stars, eight of which belong to And XVI. The RRL stars allow a new estimate of the distance, $(m - M)_0 = 23.72 \pm 0.09$ mag, which is marginally larger than previous estimates based on the tip of the red giant branch.

Key words: galaxies: dwarf – galaxies: evolution – galaxies: individual (Andromeda XVI) – Local Group – stars: variables: RR Lyrae

1. INTRODUCTION

Nearby resolved dwarf galaxies in the Local Group (LG) constitute a compelling sample to address fundamental open questions about galaxy evolution. The variety of properties in terms of mass, luminosity, surface brightness, gas content, and chemical evolution (e.g., McConnachie 2012), together with the possibility to resolve them into individual stars, offer a large number of observables to investigate how small systems evolved since their formation to the present time. In particular, the ability to derive quantitative star formation histories (SFHs) based on deep photometry reaching below the oldest main-sequence turnoff (MSTO; Gallart et al. 2005) allows us to put firm constraints on the time of the onset and of the end of star formation, which opens the possibility of constraining the physical mechanisms directly affecting the early stages of dwarf galaxy evolution. On the one hand, it is expected that both internal (supernova feedback; e.g., Mac Low & Ferrara 1999) and external mechanisms (e.g., ionizing photons from the first sources; Susa & Umemura 2004; Ricotti & Gnedin 2005) affect the star formation activity, terminating it at an early epoch. On the other hand, the environment is also expected to play a significant role on small systems orbiting massive primaries (tidal stirring, Mayer et al. 2001; ram pressure, Mayer et al. 2006; resonances, D'Onghia et al. 2009), which may have a substantial effect in stripping mass from small systems, again leading to an early cessation of the star formation.

In a series of papers, based on deep *Hubble Space Telescope* (*HST*) Advanced Camera for Surveys (ACS) photometry within the framework of the LCID collaboration (Monelli et al. 2010a, 2010c; Hidalgo et al. 2011; Skillman et al. 2014), we have shown that star formation generally continues well past $z \sim 6$ in the mass regime $M_\star \gtrsim 10^6\, M_\odot$. However, during the past 10 yr, our knowledge of the LG has been deeply influenced by

* Based on observations made with the NASA/ESA *Hubble Space Telescope*, obtained at the Space Telescope Science Institute, which is operated by the Association of Universities for Research in Astronomy, Inc., under NASA contract NAS 5-26555. These observations are associated with program #13028.
[16] Hubble Fellow.

photometric surveys that have brought about unexpected discoveries and new questions. First, the number of known LG galaxies has more than doubled in a few years only. Starting with the discovery of the first faint dwarf (also called "ultrafaint dwarfs"; Willman et al. 2005), the known satellites of the Milky Way (MW) jumped from 11 (nine bright dSph galaxies plus the Magellanic Clouds) to 50 today. These faint dwarfs extend the spectrum of galactic properties to a regime of very low mass, low luminosity, and typically low mean metallicity. They are thought to have formed stars very early on and for a very short period of time (Brown et al. 2014), possibly because cosmic reionization might have inhibited further star formation in this low-mass regime.

All currently known Local Group faint dwarfs fit well within this general trend, apart from one exception. Leo T, discovered as a stellar overdensity in the Sloan Data Release 5, immediately presented a peculiar combination of low-mass ($\sim 10^5\,M_\odot$; Ryan-Weber et al. 2008) and young stellar populations (<200 Myr; Irwin et al. 2007), together with a large fraction of H I gas (Ryan-Weber et al. 2008). Deeper *HST* data confirmed the extended star formation activity from the oldest epochs to the present day (Clementini et al. 2012; Weisz et al. 2012; see also de Jong et al. 2008), which revives the question whether cosmic reionization is the actual cause of the star formation quenching in the faintest dwarfs. Remarkably, two more galaxies recently discovered have stellar mass smaller than that of Leo T, but their color–magnitude diagrams (CMDs) show hints of extended star formation until an intermediate epoch: Eridanus II (Koposov et al. 2015; The DES Collaboration et al. 2015) and Hydra II (Martin et al. 2015), detected in the Dark Energy Survey and in the Survey for the MAgellanic Stellar History footprints.

Similarly to what occurred in the MW, the number of known satellites of M31 has increased considerably in the past few years (Martin et al. 2009; Bell et al. 2011; Richardson et al. 2011; Slater et al. 2011; Martin et al. 2013b, 2013a). This was mainly thanks to the effort of the PAndAS project (McConnachie et al. 2009). The discovery of And XVI was reported in Ibata et al. (2007), from MegaCam/CFHT observations of the M31 surroundings that later would be folded in the PAndAS survey (McConnachie et al. 2009). And XVI is located ~279 kpc from M31 in the southeast direction. The initial estimate of its luminosity ($M_V = -9.2$ mag; Ibata et al. 2007) suggested a relatively bright object. However, more recent estimates (Martin et al. 2016) revised this value to a significantly fainter value, $M_V = -7.6$ mag. First estimates based on the tip of the red giant branch (RGB) indicated a distance $(m-M)_0 = 23.60 \pm 0.2$ mag, corresponding to 525 ± 50 kpc, though smaller values have been suggested ($23.39^{+0.19}_{-0.14}$; Conn et al. 2012). Spectroscopic follow-up supports a low mean metallicity, close to [Fe/H] = −2 (Letarte et al. 2009; Collins et al. 2014, 2015). However, the most distinctive characteristic of And XVI is its extended SFH, which continued to ~6 Gyr ago (Weisz et al. 2014). The present work is part of the ISLAND project (Initial Star-formation and Lives of the ANDromeda Satellites), which obtained a total of 111 *HST* orbits to study six satellites of M31 (GO 13028, 13739): And I, And II, And III, And XV, And XVI, and And XXVIII. In this paper we present a detailed reanalysis of the data from Weisz et al. (2014), adding information on the properties of the population of variable stars and on the spatial variation of the stellar populations. In particular, Section 2 presents a brief summary of the ACS data used in this work and a detailed presentation of the And XVI CMD. In Section 3 we present the discovery and analysis of RR Lyrae (RRL) stars, and we derive a new distance for And XVI in Section 4. Section 5 is devoted to the derivation of the detailed SFH, while Section 6 presents an analysis of the variation of the properties of And XVI as a function of radius, in terms of both SFH and CMD morphology. The discussion of these results (Section 7) and a summary of the conclusions (Section 8) close the paper.

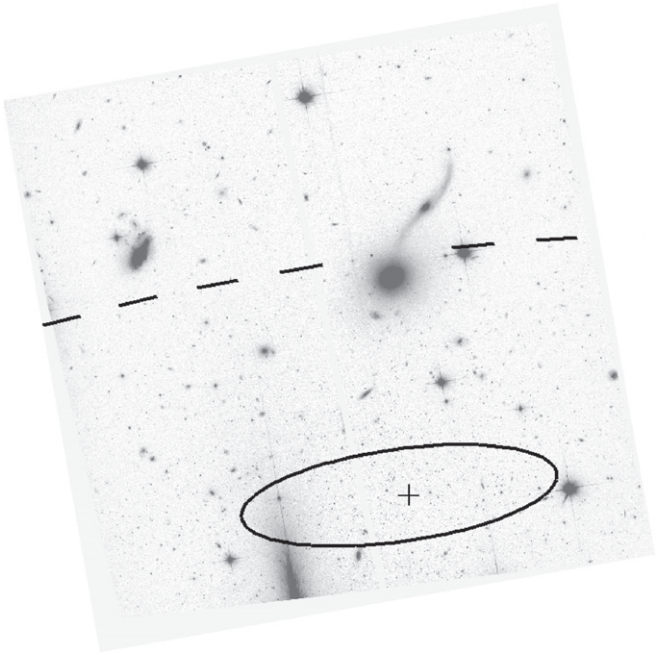

Figure 1. Stacked image of the ACS field on And XVI (north is up, east is left). A large number of extended sources are clearly visible and prompted a careful selection of the photometry list. The plus sign marks the center of And XVI, while the solid and dashed lines show the ellipses corresponding to $r_e = 1.38 r_h = 1\farcm38$, and $r_e = 5 r_h = 5\farcm00$, with r_h being the half-light radius.

2. DATA

The data set used here is the same as the one presented in Weisz et al. (2014) and consists of 13 ACS images in each of the F475W and F814W passbands. Parallel photometric reductions were conducted using both DOLPHOT and DAOPHOT/ALLFRAME, as was done for the LCID project (e.g., Monelli et al. 2010c). Here we have chosen to use the DAOPHOT/ALLFRAME photometry as a matter of convenience. The calibration to the standard VEGAMAG system was done adopting the updated zero point from the instrument Web page. Figure 1 shows a stacked drizzled image, where a large number of background extended objects are evident. In particular, note the edge-on galaxy apparently interacting with the big elliptical to the west, and the group of late-type galaxies in the northeast. The two ellipses correspond to elliptical radii $r_e = 1\farcm38$, and $5\farcm00$ and will be used in Section 6 to investigate the radial properties. Figure 2 shows the spatial distribution of the sources in the final catalog. Big colored symbols mark the position of the nine discovered RRL stars (see Section 3.1).

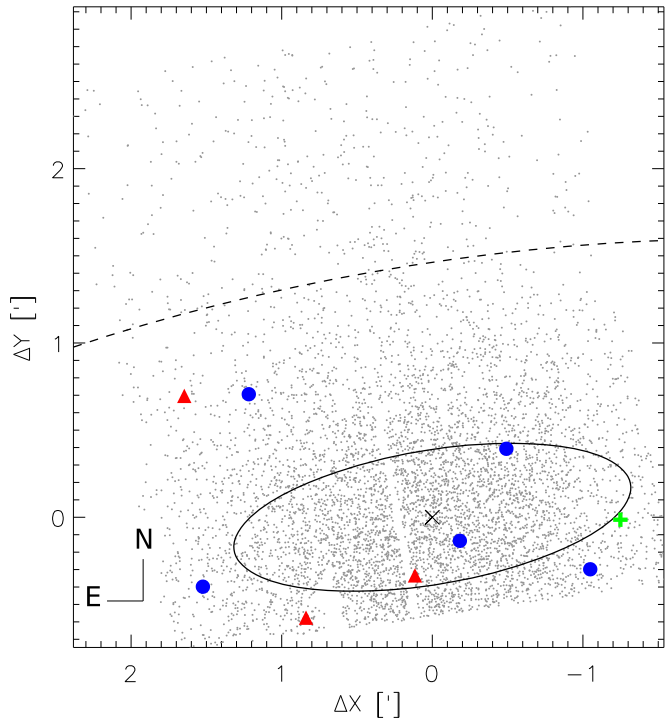

Figure 2. Spatial distribution of bona fide stellar sources in the ACS field around And XVI. The center of the galaxy is marked by the black cross. The two ellipses are the same as in Figure 1. The global SFH has been derived selecting sources within the dashed line. The location of the detected RRL variable stars is shown: red triangles mark the three RR*ab*-type stars, while blue circles represent the five RR*c*-type stars. The green plus sign marks the position of the peculiar, faint RRL star V0.

2.1. CMD Analysis

Figure 3 shows the (F475W–F814W, F814W) CMD of And XVI. In the construction of Figure 3 we adopted a reddening of $E(B-V) = 0.06$ (Schlafly & Finkbeiner 2011) and a distance modulus of $(m - M)_0 = 23.72$ mag. The latter value has been derived from the RRL stars, as detailed in Section 4.1. The RRLs discovered in And XVI are plotted as large symbols and will be discussed in Section 3.

A photometric selection was applied according to the sharpness parameter provided by DAOPHOT ($|\mathrm{sharp}| < 0.3$). Given the small number of And XVI stars and the heavy contamination from background galaxies, we performed a further check on the stacked image, removing a few hundred sources associated with extended objects and spikes of heavily saturated field stars. Finally, we ended up retaining 5714 bona fide stellar sources within the 5.′0 ellipse. These are shown in the CMD of the left panel, where the typical features of a predominantly old stellar population clearly appear. The RGB spans more than five magnitudes, from the tip at F814W $\approx$ 20 mag down to F814W $\approx$ 25.5. The horizontal branch (HB) has a predominantly red morphology with a well-populated red part, concentrated close to (F475 W− F814W, F814W) $\sim$ (1.2, 23.5) mag, which is well separated from the RGB, suggesting a limited metallicity spread. On the other extreme, the HB extends to the blue, reaching well beyond the RRL instability strip to F475 W− F814W $\sim$ 0.2 mag. Overall, we derive an HB morphology index $= -0.64$.[17]

The middle panel of the same figure shows the comparison with selected isochrones from the BaSTI[18] stellar evolution library (Pietrinferni et al. 2004, 2009). In particular, the red and green lines represent an old (13 Gyr, $Z = 0.0001$) and a not-too-old (6 Gyr, $Z = 0.0003$; Castellani & degl'Innocenti 1995) population. These two isochrones bracket both the RGB and the MSTO region well. Interestingly, this suggests that the stellar populations in And XVI are characterized by a considerable age spread, but a small range of metallicities.

Finally, the right panel presents the sources detected in the outermost region of the field of view, for $r_e > 5'$. The same old isochrone as in the middle panel is shown. Roughly 400 sources are present in this diagram, but no obvious features appear. Many of the detected objects present colors redder than the MS stars of And XVI, suggesting that they are unresolved background galaxies. Neverthless, we cannot rule out the possibility that some And XVI stars are still present in this region, which will be anyway excluded from the SFH analysis.

2.2. Blue Straggler Stars

The CMD clearly shows a plume of objects bluer and brighter than the old MSTO, between F814W $\sim$ 25.5 mag and F814W $\sim$ 27.5 mag. They are most likely blue straggler stars (BSSs) formed by primordial binary stars, as commonly found in many dSph galaxies (Mapelli et al. 2007, 2009; Monelli et al. 2012; Santana et al. 2013). On the other hand, stars in that region of the CMD might be genuine young objects, with ages in the range between $\sim$1 and $\sim$3 Gyr. The blue line in Figure 3 represents a metal-poor isochrone of 2.5 Gyr, which provides a fair agreement with the observed sequence. If And XVI hosted such a young population, one would expect to find it spatially concentrated in the innermost region of the galaxy, as commonly observed in LG dwarfs. Figure 4 shows the cumulative distribution of stars in the blue plume, the RGB, and the HB. Within the error, they are identical as a function of elliptical radius. This indirectly supports the inference that the stars in the blue plume are BSSs and not a young population. The plume of blue objects causes a minor peak in the SFH between 2 and 3 Gyr ago (Section 5.2), which contributed $\sim$3% of the stellar mass. Both the age range and the mass percentage are consistent with those estimated in Cetus and Tucana (Monelli et al. 2012). This again indirectly supports the BSS hypothesis.

3. VARIABLE STARS

Our observational strategy was designed for optimal time sampling of short-period ($\lesssim$1 day) variable stars such as RRL and anomalous Cepheids (ACs). All the observations were executed within $\sim$2.1 days and were organized in six visits, five of two orbits and one of three orbits. Moreover, each orbit was split into one F475W and one F814W exposure, and a sequence F475W–F814W–F814W–F475W was observed in each group of two visits. This allowed a larger time difference between the two images at shorter wavelength, where the amplitude is larger. Table 1 reports the observation log, listing the image name, filter, exposure time, starting date of observation, and modified Julian date at midexposure.

[17] The HB index was introduced by Lee (1990), and it is defined as HBR $= (B\text{-}R)/(B + V + R)$, where B and R are the number of HB stars bluer and redder than the instability strip, respectively, and V is the total number of RRL stars.

[18] http://basti.oa-teramo.inaf.it/index.html

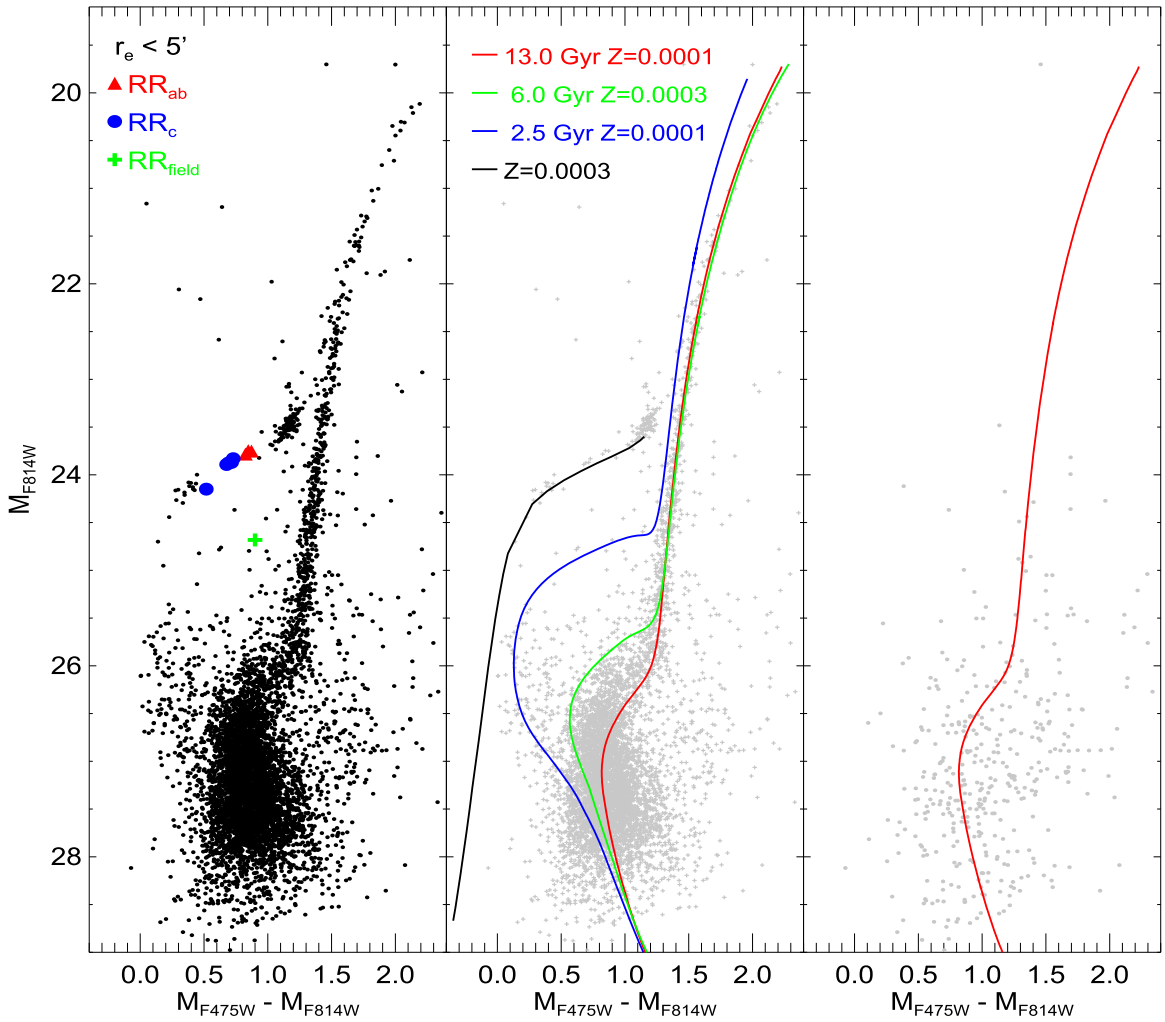

Figure 3. Left: CMD of And XVI, spanning from the tip of the RGB to well below the MSTO. Colored symbols show the RRL stars, with the same color code as in Figure 2. Middle: same CMD with superimposed selected isochrones from the BaSTI database, for labeled age and metallicity. The two selected isochrones bracket completely the TO region and the color spread of the RGB, suggesting a significant spread both in age and in metallicity. The black line shows the zero-age HB for $Z = 0.0003$, which nicely reproduces the lower envelope of the HB stars. Right: CMD of the outermost region in the field of view, for $r_e > 5'$, where the majority of the detected sources are polluting unresolved background galaxies.

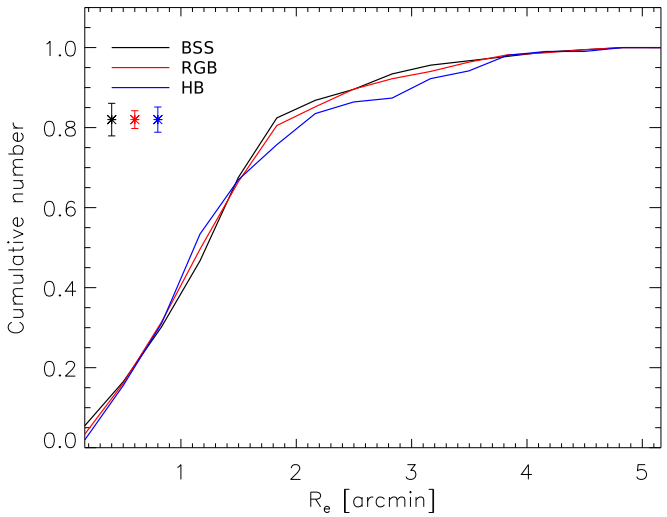

Figure 4. Normalized cumulative radial distribution of stars in the RGB stars, HB stars, and the candidate BSSs. Within the error, no significant differences are detected.

3.1. RRL Stars

Candidate variable stars were identified following the same approach adopted for the galaxies of the LCID project (Bernard et al. 2009, 2010, 2013). In particular, we used the variability index introduced by Stetson (1996). The light curves of selected candidates were individually visually inspected, and nine variables were confirmed. Given their pulsational properties and the location on the CMD, we classify all of them as RRL stars. The F475W and F814W magnitudes were recalibrated to the Johnson *BVI* system using the same relations adopted in Bernard et al. (2009). Table 2 summarizes the properties of the confirmed variables, which are named in order of increasing R.A. Their position in the CMD is shown in Figure 3: red triangles and blue circles represent RR*ab*- and RR*c*-type stars, respectively. Interestingly, one variable (V0) is significantly fainter (green plus sign), by ∼0.8 mag in the F814W band. Figure 5 presents the light curves of the nine variables. Despite the small number of phase points, the time sampling chosen when preparing the observations provides a fairly homogeneous coverage of the light curves. In particular, we do not find any obvious problem with V0 that may account

Table 1
Log of the Observations

Image Name	Filter	Exp. Time (s)	Date (UT Start)	MJD d-2,400,000
jc1d09upq	F475W	1280	2013 Nov 20 12:46:13	56616.545139
jc1d09urq	F814W	987	2013 Nov 20 13:10:30	56616.560301
jc1d09uuq	F814W	1100	2013 Nov 20 14:13:37	56616.604792
jc1d09uyq	F475W	1359	2013 Nov 20 14:34:55	56616.621076
jc1d10wdq	F475W	1280	2013 Nov 20 23:55:40	56617.010037
jc1d10wfq	F814W	987	2013 Nov 21 00:19:57	56617.025199
jc1d10xaq	F814W	1100	2013 Nov 21 01:23:05	56617.069701
jc1d10xeq	F475W	1359	2013 Nov 21 01:44:23	56617.085986
jc1d11ywq	F475W	1280	2013 Nov 21 09:29:27	56617.408499
jc1d11yyq	F814W	987	2013 Nov 21 09:53:45	56617.423673
jc1d11z1q	F814W	1100	2013 Nov 21 10:56:55	56617.468199
jc1d11z5q	F475W	1359	2013 Nov 21 11:18:13	56617.484483
jc1d12a2q	F475W	1280	2013 Nov 21 15:52:01	56617.674172
jc1d12a5q	F814W	987	2013 Nov 21 16:16:18	56617.689334
jc1d12a9q	F814W	1100	2013 Nov 21 17:23:30	56617.736660
jc1d12zzq	F475W	1359	2013 Nov 21 17:44:48	56617.752522
jc1d13b9q	F475W	1280	2013 Nov 21 23:50:12	56618.006245
jc1d13bbq	F814W	987	2013 Nov 22 00:14:29	56618.021407
jc1d13caq	F814W	1100	2013 Nov 22 01:17:39	56618.065933
jc1d13ceq	F475W	1359	2013 Nov 22 01:38:57	56618.082218
jc1d14f2q	F475W	1280	2013 Nov 22 10:59:39	56618.471143
jc1d14f4q	F814W	987	2013 Nov 22 11:23:56	56618.485872
jc1d14f7q	F814W	1100	2013 Nov 22 12:27:08	56618.530854
jc1d14fbq	F475W	1359	2013 Nov 22 12:48:26	56618.547139
jc1d14feq	F475W	1360	2013 Nov 22 14:02:46	56618.598771
jc1d14fiq	F814W	1100	2013 Nov 22 14:28:23	56618.615056

for the fainter magnitude, though the light curve is admittedly noisy. We have checked whether a significantly higher metal content may be responsible for such a lower luminosity. Adopting the luminosity–metallicity relation by Clementini et al. (2003), we derive that an [Fe/H] approximately solar is required to explain such a large magnitude difference. Such a large metallicity spread within the population of stars able to form RRL in And XVI looks unlikely, in particular if we take into account the relatively small range estimated both spectroscopically (Letarte et al. 2009; Tollerud et al. 2012) and with the SFH (see Section 5.2). Alternatively, we can assume that V0 does not belong to And XVI and the magnitude difference is due to a distance effect. Assuming a metal content of [Fe/H] $= -1.9$ and the metallicity–luminosity relation from Clementini et al. (2003; see Section 4.1), we derive a distance difference between V0 and the rest of the variables of the order of ∼290 kpc. Given that And XVI is located ∼200 kpc closer than M31, this means that V0 is compatible with being located ≈100 kpc beyond M31, but still well within its virial radius, thus being a possible candidate M31 halo star (Ibata et al. 2014).

Figure 6 shows the period–amplitude (Bailey) diagram for the detected variable stars. The dotted and dashed lines mark the loci of Oosterhoff I and Oosterhoff II globular clusters, respectively, from Cacciari et al. (2005). The solid line is the locus defined for RR*c* stars, from Kunder et al. (2013). The three And XVI RR*ab* stars occupy the region intermediate to the two curves. However, both the mean period of RR*ab* stars ($\langle P_{ab} \rangle = 0.636$ days) and that of the RR*c* type ($\langle P_c \rangle = 0.357$ days) are close to the typical values for the Oosterhoff II type stellar systems. Note that the ratio between the number of RR*c* and RR*ab* is unusually large (Catelan 2009), and And XVI is the only dwarf known with more RR*c* than RR*ab*. This finding is particularly intriguing given the red morphology of the HB, which would favor the sampling of the red part of the instability strip, where the RR*ab* are located. However, it might be possibly related to the small total number of RRL stars. Alternatively, this effect could be related to the low metallicity of the oldest stars, such as the RRL stars, which would be preferentially located in the blue part of the HB. However, we note that for other M31 satellites with a similar small number of RRL variables and bluer HB morphology such as And XI and And XIII (Yang & Sarajedini 2012), the number of RR*ab*-type stars is larger than that of RR*c* type (10 versus 5 and 8 versus 1, respectively).

3.2. Anomalous Cepheids

We report that we did not discover any ACs in the surveyed area of And XVI. These kinds of pulsating variables, present only in metal-poor ($Z < 0.0006$; Fiorentino et al. 2006) populations, are centrally He-burning stars typically ∼1 mag brighter than RRL stars. They can form through two different channels: (i) single, evolved stars of mass $1.3\ M_\odot \lesssim M \lesssim 2.2\ M_\odot$, therefore younger than ∼1 Gyr; and (ii) coalescent binary stars evolved after the BSS phase. Despite the fact that ACs have been observed in many dSph galaxies (Sculptor, Kaluzny et al. 1995; Fornax, Bersier & Wood 2002; Carina, Dall'Ora et al. 2003; Coppola et al. 2013; Draco, Kinemuchi et al. 2008; Cetus and Tucana, Bernard et al. 2009), the nondetection in And XVI is not surprising, and we ascribe it to its low mass. First, the lack of ACs agrees with the lack of recent star formation, thus excluding the first formation channel. Second, the small number of stars populating the blue plume of BSS (∼230) implies that very few evolved stars

Table 2
Variable Star Properties

Name	R.A. (h m s)	Decl. (° ′ ″)	Type	P (day)	m_{F475W} (mag)	A_{F475W} (mag)	m_{F814W} (mag)	A_{F814W} (mag)	m_B (mag)	A_B (mag)	m_V (mag)	A_V (mag)	m_I (mag)	A_I (mag)
V0	00:59:24.38	32:22:33.14	*ab*	0.622	25.582	0.889	24.682	0.431	25.727	0.990	25.244	0.767	24.670	0.446
V1	00:59:25.33	32:22:16.09	*c*	0.358	24.568	0.641	23.875	0.399	24.681	0.725	24.328	0.538	23.857	0.397
V2	00:59:27.97	32:22:57.56	*c*	0.391	24.560	0.557	23.831	0.284	24.668	0.616	24.308	0.454	23.812	0.290
V3	00:59:29.43	32:22:25.88	*c*	0.350	24.569	0.541	23.892	0.358	24.667	0.573	24.325	0.480	23.873	0.361
V4	00:59:30.84	32:22:13.99	*ab*	0.617	24.623	0.840	23.751	0.589	24.741	0.969	24.313	0.810	23.735	0.600
V5	00:59:34.27	32:21:59.43	*ab*	0.638	24.594	1.200	23.747	0.655	24.717	1.182	24.323	0.978	23.731	0.667
V6	00:59:36.07	32:23:16.33	*c*	0.399	24.586	0.444	23.870	0.216	24.694	0.478	24.342	0.390	23.851	0.217
V7	00:59:37.51	32:22:10.07	*c*	0.288	24.668	0.300	24.150	0.161	24.736	0.316	24.495	0.251	24.134	0.157
V8	00:59:38.10	32:23:15.76	*ab*	0.651	24.608	0.673	23.783	0.427	24.734	0.719	24.327	0.574	23.767	0.432

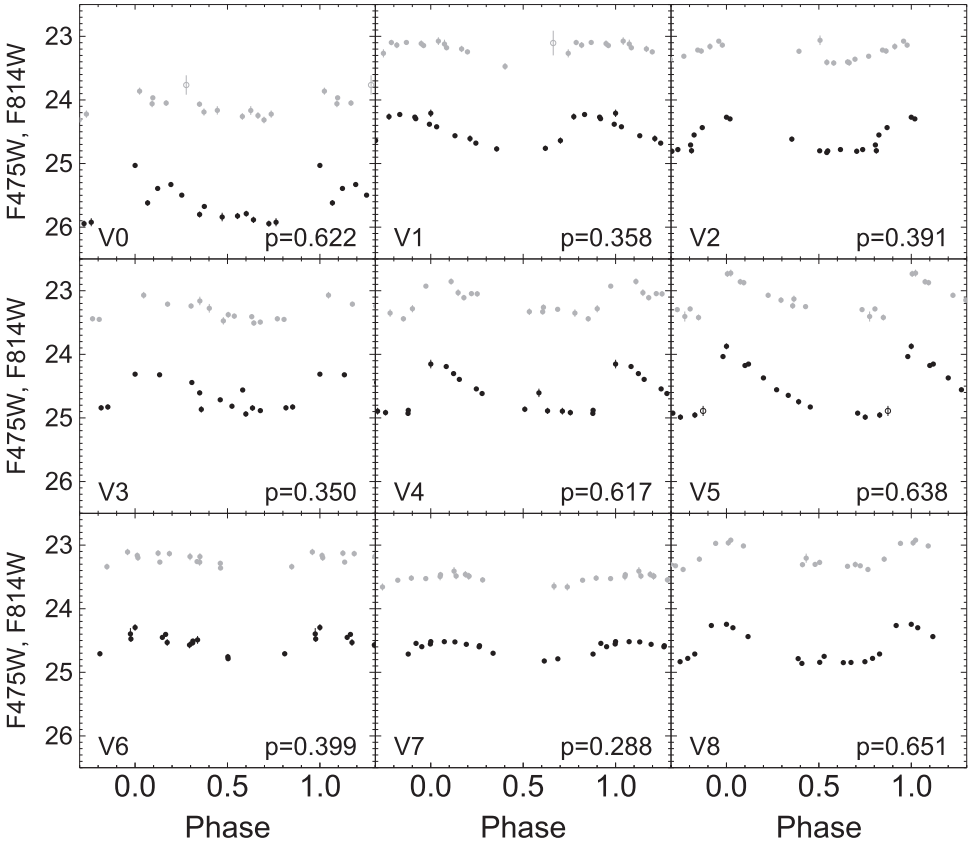

Figure 5. Light curves of the nine discovered RRL stars. In each panel, black and gray points refer to the F475W and F814W data. For the sake of clarity, F814W was shifted by −0.6 mag to avoid overlap. Open points are excluded from the light-curve fit owing to large photometric error. Note that V0 is significantly fainter than the other eight RRL stars, compatible with an M31 field variable.

of this population are expected. These, owing to their mass, tend to occupy the red part of the HB, at temperatures lower than the instability strip, and few such stars are clearly visible above the red HB, at F814 W $\sim$ 23 mag. Finally, adopting the relation between the frequency of ACs and the luminosity of the host galaxy, discovered by Mateo et al. (1995) and updated by Fiorentino & Monelli (2012), we estimate that 1 $\pm$ 1 ACs are expected in the surveyed area, in agreement with the current observations.

4. DISTANCE ESTIMATE

4.1. RRL Distance Estimate

Pulsational properties of RRL stars can be used to derive a robust estimate of the distance. In the following we will use three different methods. In the analysis, we did not include the faint V0 RRL star.

a.First, we adopt the relation between the intrinsic luminosity, M_V, and the metallicity. In the range below [Fe/H] = −1.6 we assume two linear relations[19]:

$$M_V(\mathrm{RR}) = 0.866(\pm0.085) + 0.214(\pm0.047)[\mathrm{Fe/H}] \quad (1)$$

from Clementini et al. (2003) and

$$M_V(\mathrm{RR}) = 0.72(\pm0.07) + 0.18(\pm0.07)[\mathrm{Fe/H}] \quad (2)$$

[19] The F475W and F814W magnitudes were recalibrated to the Johnson *BVI* system using the same relations adopted in Bernard et al. (2009).

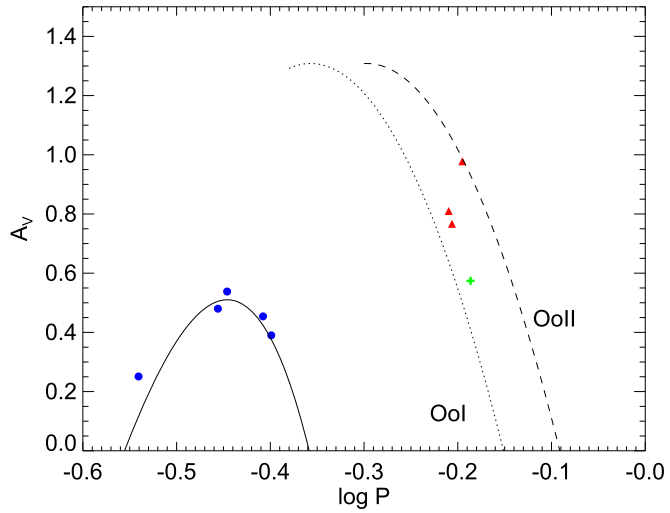

Figure 6. Period–amplitude (Bailey) diagram for the nine detected variables. The dotted and dashed lines are the loci of RRL stars in Oosterhoff I and Oosterhoff II type globular clusters, respectively, from Cacciari et al. (2005). The solid line is the analogous curve for RR*c* type from Kunder et al. (2013).

from Bono et al. (2003). We assume a value for the [Fe/H] = −2, in agreement with the available spectroscopic measurements (Letarte et al. 2009; Collins et al. 2014, 2015). For the metal content, the Clementini et al. (2003) and the Bono et al. (2003) relations provide absolute magnitude values of $M_V = 0.438$ and 0.360 mag, respectively. We derive absolute distance moduli for And XVI, corrected for extinction, of $(m - M)_0 = 23.72 \pm 0.09$ mag and 23.79 ± 0.08 mag, respectively, corresponding to 554 and 572 kpc. We note that a change in the metal content by 0.2 dex affects the distance estimates by ∼0.04 mag.

b.It is well established that RRL stars obey a period–luminosity–metallicity relation in the near-infrared, which can be expressed in the form

$$\mathrm{Mag} = a + b[\mathrm{Fe/H}] + c\mathrm{Log}P. \quad (3)$$

We adopt here the most updated theoretical relations from Marconi et al. (2015), for both the Wesenheit W(I, $B - I$) and W(I, $V - I$) magnitudes.

We used here the full sample of RRL stars after fundamentalizing the RR*c* type by adding 0.127 to the logarithm of their period. We calculated the Wesenheit apparent magnitudes of each star, and adopting these relations, we derived the true distance modulus. Assuming [Fe/H] ∼ −2.3 dex ($Z \sim 0.0001$), the two relations provide $(m - M)_0 = 23.74 \pm 0.03$ mag and $(m - M)_0 = 23.77 \pm 0.06$ mag, respectively. A slightly larger metallicity, [Fe/H] ∼ −1.8 dex (Z ∼0.0003), shortens the derived distance by a few hundredths of a magnitude: $(m - M)_0 = 23.68 \pm 0.03$ mag and $(m - M)_0 = 23.70 \pm 0.03$ mag.

c.An independent method to derive the distance based on the RRL properties was introduced by Caputo et al. (2000) and takes advantage of the period–luminosity–metallicity relation at the first-overtone blue edge of the instability strip. Ideally, this method works well if the blue side of the instability strip is well sampled, which is not the case for the current data set. However, the few RR*c*-type stars found can provide an upper limit to the distance. Applying the relations from Caputo et al. (2000) to the shortest-period star, we derive a distance modulus of 23.83 ± 0.07, again assuming [Fe/H] = −2.

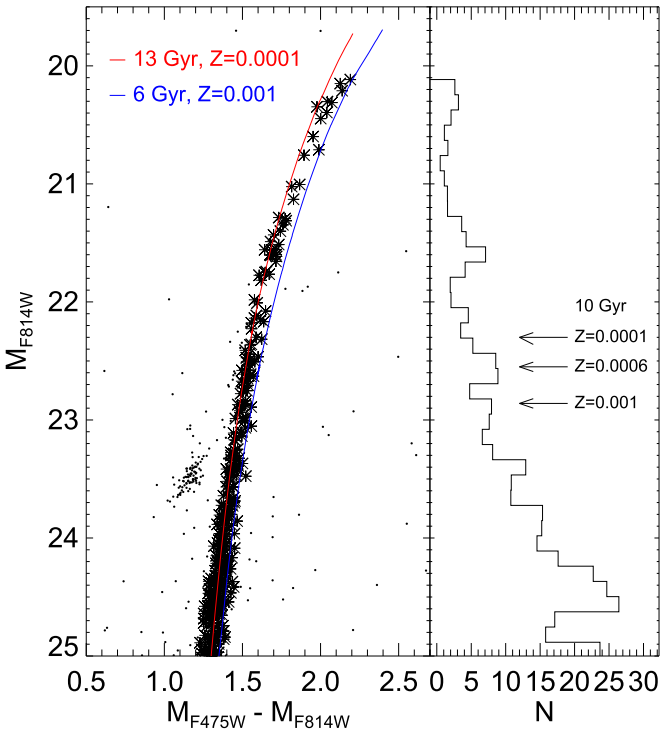

Figure 7. Left: CMD of And XVI showing the RGB stars (asterisks) used to detect the RGB tip. Two isochrones are also overplotted: $Z = 0.0001$, $t = 13$ Gyr (red line), and $Z = 0.001$, $t = 6$ yr (blue line). We assumed $(m - M)_0 = 23.72$ mag and $E(B - V) = 0.06$ mag. Right: luminosity function of RGB stars. The three arrows mark the expected position of the RGB bump for three isochrones of 10 Gyr: $Z = 0.0001$, $Z = 0.0006$, and $Z = 0.001$.

Overall, these different methods applied to the RRL star sample of And XVI provide consistent results about its distance. For consistency with previous analysis of isolated galaxies within the framework of the LCID project, we will adopt the distance derived with the M_V–[Fe/H] relation by Clementini et al. (2003), $(m - M)_0 = 23.72 \pm 0.09$ mag, to derive the SFH in Section 5.

4.2. RGB Tip Distance Estimate

Ibata et al. (2007) estimated the distance of And XVI to be $(m - M)_0 = 23.6 \pm 0.2$ mag (525 Kpc), based on the position of the tip of the RGB. A more recent study by Conn et al. (2012), based on a more sophisticated analysis of the same feature, suggested a slightly shorter distance, $(m - M)_0 = 23.39^{+0.19}_{-0.14}$ (476 kpc). We note that the distance estimates based on the RRL stars are systematically larger than those based on the tip of the RGB. However, they are still in agreement, within the error bars, with the value provided by Ibata et al. (2007), and only in marginal agreement at the 2σ level with the measurement by Conn et al. (2012).

Figure 7 summarizes our attempt to derive a distance to And XVI based on tip of the RGB as detected in the ACS data. The left panel shows a zoom-in of the CMD in the RGB region, and the right panel presents the luminosity function of RGB stars in the F814W band. These are highlighted by big asterisks in the left panel. The plot clearly shows that the region of the RGB tip is heavily undersampled, with only nine stars detected in the half brightest magnitude. This is far from the at least 50 stars

recommended by Madore & Freedman (1995) to derive a distance modulus with 0.1 uncertainty. This is also supported by the comparison with theoretical isochrones (red line: $Z = 0.0001$, $t = 13$ Gyr; blue: $Z = 0.001$, $t = 6$ Gyr). Assuming $(m-M)_0 = 23.72$ mag (from the RRL estimate; see Section 4.1), it is evident that the brightest portion of the RGB is devoid of observed stars. Note that a shorter distance modulus would move the isochrones to brighter apparent magnitudes, thus worsening the problem. Given the little contamination from both And XVI AGB and foreground field stars, we can set an upper limit to the distance, assuming that the brightest observed star is representative of the tip. This has magnitude F814W = 20.116 mag. The F814W absolute magnitude of the RGB tip shows a mild dependence on the metallicity in the metal regime appropriate for the stars in And XVI. In more detail, theoretical predictions based on BaSTI stellar models show that $M^{\rm tip}_{\rm F814W}$ is equal to −4.087 at $Z = 0.0001$ and to −4.166 for $Z = 0.001$. When combining these model predictions with an extinction estimate of $A_{\rm F814W} = 0.11$ mag, we obtain a distance modulus upper limit ranging from 24.09 to 24.17 mag, i.e., in the range 657–682 kpc. A visual inspection of the CMD from Ibata et al. (2007) discloses that at least one very bright star is missing in our photometry, possibly because it is outside our field of view. This is probably what causes the difference in the derived distance using the same approach. In any case, it is evident that the poor statistics in the RGB star counts are strongly hampering the possibility to use the RGB tip method for a robust distance estimate.

In passing, we note that for the same reason, no clear detection of the RGB bump is possible. The luminosity function in the right panel of Figure 7 does not show any clear evidence of the RGB bump. The three overplotted arrows mark the position of the RGB bump derived from theoretical isochrones of 10 Gyr and metallicity ranging from $Z = 0.0001$ to $Z = 0.001$. We note that an observed peak around F814 W ∼ 22.5 mag agrees well with the predicted bump for $Z = 0.0006$ and age of 10 Gyr. As the bump positions depend on both the age (fainter bump for increasing age) and the metallicity (fainter bump for increasing metallicity), there is some degree of degeneracy. However, it seems clear that the observed peak cannot be reproduced with very metal-poor populations, as the predicted bump for $Z = 0.0001$ and an age of 10 Gyr is too bright (F814 W ∼ 22.35 mag) and gets brighter for decreasing age, while it is virtually undetectable for older ages, as the magnitude extension of the loop drops. Similarly, in the case of more metal-rich populations, the predicted bump is too faint, and an age of 6 Gyr is required to fit the observed peak (though with a color that is too red).

5. STAR FORMATION HISTORY

5.1. SFH Derivation

The SFH was derived using the IAC-star, MinnIAC, and IAC-pop codes (Aparicio & Gallart 2004; Aparicio & Hidalgo 2009; Hidalgo et al. 2011), in a similar fashion to that already presented in previous papers of the LCID project (Monelli et al. 2010a, 2010c; Hidalgo et al. 2011; Skillman et al. 2014). For the present data set, we used a model CMD of 3×10^6 stars with ages and metallicities uniformly distributed in the ranges $0 < t < 13.5$ Gyr and $0.0001 < Z < 0.0025$. Observational errors were simulated taking into account the results of 2×10^6 artificial stars.

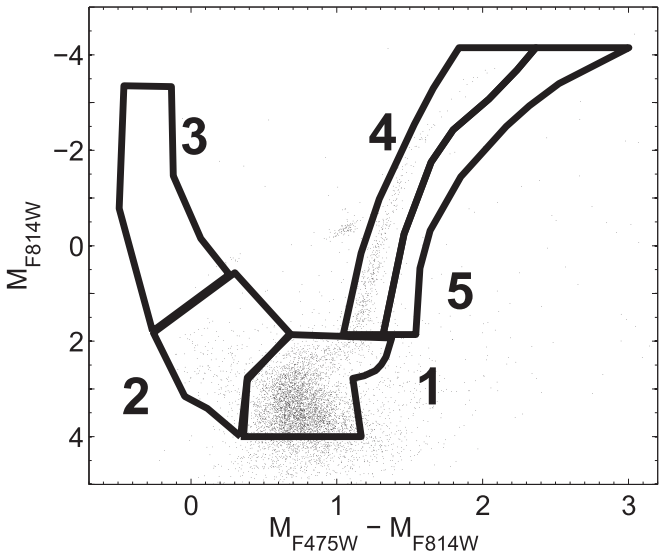

Figure 8. CMD of And XVI with the five regions (*bundles*) used to derive the SFH superimposed. See text for details.

IAC-star requires the selection of a number of parameters that are used in the solution derivation. On the one hand, parameters used to build the model CMD such as the number of binary stars and the initial mass function (IMF) were chosen to be the same as in previous LCID papers. Namely, we used a 40% binary faction ($q > 0.5$) and the Kroupa (2002) IMF ($x = 1.3$ for $M < M_\odot$ and $x = 2.3$ for $0.5 < M_\odot < 100$). To run IAC-pop and MinnIAC, decisions have to be taken concerning the parameterization of both the age and metallicity bins (which define the "simple stellar populations") and that of the CMDs. The adopted age and metallicity bins were as follows: age = [0 1 2.5:1:13.5] Gyr, metallicity = [0.0001 0.0003 0.0005 0.0007 0.0010 0.0015 0.0020 0.0025]. The sampling of the CMD is based on macroregions, called *bundles* (see Figure 8). In each bundle, stars are counted in a regular grid of boxes, whose size is fixed and constant. The main limit of the current data set is the relatively small number of stars in the observed CMD, which can introduce noise in the solution if too fine of a sampling of the CMD is adopted. Therefore, we performed a number of tests to optimize the bundle and box sizes. We found that the final solution is mostly affected by two factors: (i) the sizes of the boxes in *bundle 1*, and (ii) the inclusion of the RGB in *bundle 4*.

Most of the information on the age of the stellar population comes from the MSTO region. For predominantly old populations such as those present in And XVI, most of the information will come from *bundle 1*. *Bundle 3* and *bundle 5* are useful to set limits to the youngest populations and the highest metallicity, respectively, while *bundle 2* samples the blue plume. In previous works, in order to give more weight to the TO region, we adopt smaller boxes in the corresponding bundle. However, we found that, in comparison with our previous LCID experience, we had to significantly increase the size of individual boxes in this bundle in order to avoid fluctuations and the appearance of spurious populations in the solution. Namely, the box size chosen is (color, magnitude) = (0.04, 0.2) mag, compared to typically (0.02, 0.1) in

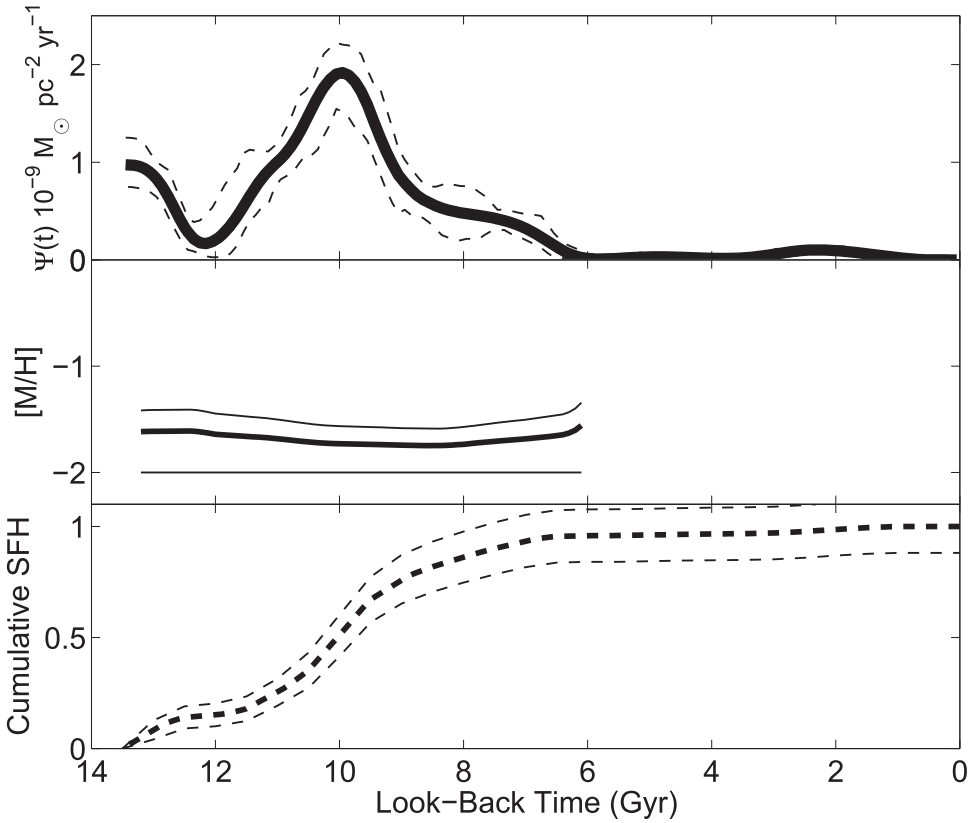

Figure 9. SFH of And XVI. As a function of lookback time, from top to bottom the three panels show the SFR, the AMR, and the cumulative SFH. Clearly, And XVI was able to sustain star formation for at least 6 Gyr.

LCID. Given the little or negligible number of stars, larger boxes are used in bundles 2, 3, and 5. The HB is excluded from the SFH analysis because the details of its morphology depend on highly unknown factors such as the mass loss during the RGB phase, and they are not properly modeled in our synthetic CMD.

The second major difference with the LCID strategy is that including the RGB significantly improves the solution as well. With the LCID galaxies we had demonstrated that, whenever the CMDs are well populated by at least tens of thousands of stars, the inclusion of the RGB has little, if any, effect on the final solution, and typically the χ^2 increases (Bernard et al. 2012). This is mostly due to the fact that the age is highly degenerate in the RGB, while a bundle such as the current *bundle 5* is always useful to set a constraint to the most metal-rich population. In the current analysis, where only a few thousand stars are available, we found that the solution strongly benefits from the inclusion of a bundle on the RGB. The main effect is that spurious populations (such as simultaneously very old and very metal-rich ones) disappear from the solution.

5.2. Global SFH of And XVI

The SFH of And XVI was derived using only stars within $5r_h$ from the center. The total number of stars used to derive the SFH is 3985, 202, and 491 in *bundles 1*, *2*, and *4*, respectively. For larger galactocentric distances, the majority of sources are expected to be background unresolved galaxies. Nevertheless, the comparison with theoretical isochrones in Figure 3 suggests that a small fraction of And XVI stars may be present at larger radius. Scaling the number of objects in the outer regions found in the same bundles within $5r_h$, we find that an upper limit of ∼4.5% of contaminating objects may be affecting the star counts, thus not strongly affecting the derived SFH. In particular, since the distribution of the contaminating galaxies in the CMD does not resemble that of a stellar population, we do not expect that they originate any strong features at a specific age in the SFH.

The final solution is presented in Figure 9. The three panels represent, from top to bottom, the star formation rate (SFR), the age–metallicity relation (AMR), and the cumulative SFH as a function of the lookback time. And XVI is populated by both old and intermediate-age stars. It started forming stars at the oldest possible epoch. Remarkably, in our SFH solutions, there appears to be a significant very old peak at 13.5 Gyr ago, followed by a sudden drop of star formation. After a minimum occurred 12 Gyr ago, star formation increased again and reached its peak ∼10 Gyr ago. This is an extremely interesting finding, as this feature is not common among either the MW dSph satellites or the isolated ones such as Cetus and Tucana. In fact, they typically present one single dominant event of star formation that occurred at the oldest epochs (see, e.g., Monelli et al. 2010c, 2010b; de Boer et al. 2012a, 2012b). The second distinctive feature we recover, as already found by Weisz et al. (2014), is that the star formation activity extends for many Gyr, vanishing 6 Gyr ago. The blue plume of stars in *bundle 2* produces the small peak at ∼3 Gyr, which we interpret as BSSs (see Section 2.2). We also recover a fundamentally constant AMR, with metallicity not exceeding [M/H] = −1.5 (Z = 0.0006), in agreement with the qualitative comparison with theoretical isochrones. Further constraining the nature of the cumulative SFH reveals that 10% of And XVI stellar mass

Table 3
Integrated and Mean Quantities

Quantity	Value
$\int \langle \Psi(t) \rangle dt$ ($10^6 M_\odot$)	1.92 ± 0.03
$\langle \Psi(t) \rangle$ ($10^{-8} M_\odot$ yr^{-1} pc^{-1})	3.6 ± 0.1
$\langle$age$\rangle$ (Gyr)	9.9 ± 0.1
$\langle$[Fe/H]$\rangle$ 10^{-4} dex	4.2 ± 0.1

was in place by $z \sim 6$ (∼12.8 Gyr ago), which is when the reionization epoch concluded, and that And XVI formed 50% of its stellar mass by $z \approx 2$, or ∼10.1 ± 0.2 Gyr ago (see Table 3 for the derived integrated and mean quantities).

Figure 10 presents a comparison between the SFH recovered using different photometry sets and stellar evolution libraries. In particular, together with the previous DAOPHOT+BaSTI solution (black lines), we show the SFH obtained with DAOPHOT+Girardi (red lines; Girardi et al. 2000) and DOLPHOT+BaSTI (gray lines). The figure presents both the SFR as a function of time (top panel) and the normalized cumulative SFH (bottom). The plots disclose a general very good agreement. In particular, the three solutions confirm the fundamental results that the star formation in And XVI did extend to ∼6 Gyr ago, and that there is no dominant initial event as in other dSph galaxies such as Cetus and Tucana. We exclude that this can be an artifact due to photometric errors, as they are too small to affect the TO morphology causing the age spread, in either photometry. Moreover, the three solutions confirm an initial star formation followed by a less intense activity. In particular, the use of either photometry set, together with the BaSTI models, provides a minimum at 12 Gyr, while the subsequent maximum is 1 Gyr younger in the DOLPHOT +BaSTI solution than in the DAOPHOT+BaSTI one. Interestingly, while the BaSTI solution provides a strong peak at such ages, the solution based on the Girardi library is characterized by a flatter SFR, though the age of the peaks agrees very well with the BaSTI solutions. The consistency between the three solutions is clear in the bottom panels, where the cumulative SFHs agree at the 1σ level.

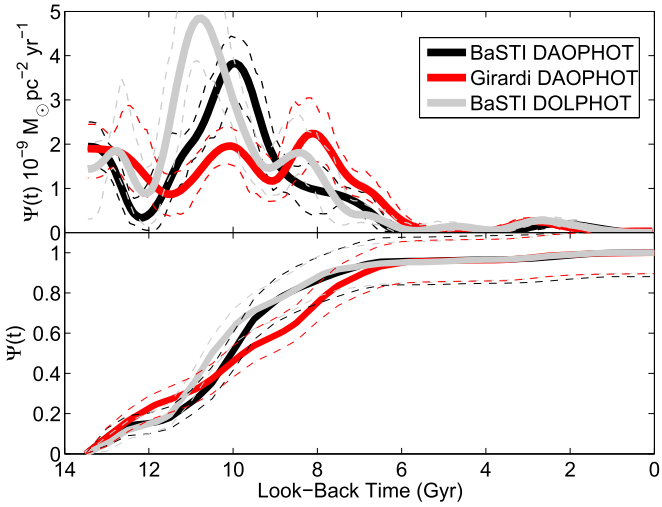

Figure 10. SFH solutions obtained adopting different photometry sets and different stellar evolution libraries. The top panel shows the SFR as a function of time, while the bottom panel presents the normalized cumulative SFH.

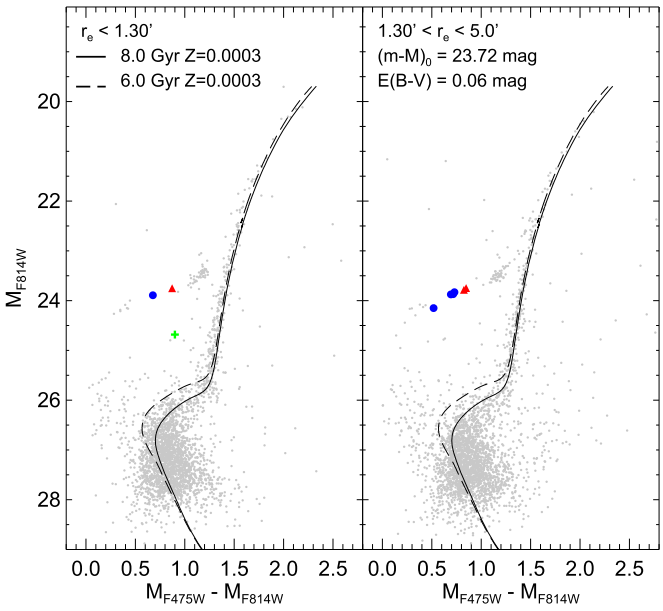

Figure 11. CMDs of the inner ($r_e < 1\farcm38$; left) and outer regions ($1.3 \geqslant r_e < 5\farcm00$; right) of And XVI. Color symbols show the RRL stars in each region. The separation between the inner and outer region is such that the two CMDs contain the same number of sources within the *bundles*. Two not-too-old isochrones are overplotted ($Z = 0.0003$, $t = 6$, 8 Gyr). The number of stars in the TO region composed by the two curves is larger in the inner than in the outer region, suggesting stronger star formation at this age closer to the center of the galaxy.

6. RADIAL SPATIAL GRADIENT

In this section we investigate how the properties of And XVI change as a function of the distance from its center. First, we note that we do not have a symmetric spatial sampling of the galaxy. In fact, owing to a bright field star next to the innermost regions of And XVI, we were forced to point the telescope such that the center of the galaxy is next to the edge of the ACS camera, at (X, Y) ≈ (566, 1847) pixels (see the black cross in Figure 2). Second, we estimate that the current ACS data cover ≈23% of the galaxy area.

For the following analysis, we take advantage of a homogeneous derivation of the structural parameters of all M31 dwarf spheroidal galaxies that fall in the PAndAS footprint (Salomon et al. 2015) and use the following, updated values for the centroid (0:59:30.3 + −0.4; +32:22:34 + −0.4), ellipticity (0.29 ± 0.08), position angle (98° ± 9°), and half-density radius (1′.0 ± 0′.1). We calculated the elliptical distance for each star from the galaxy center, and we used it to select three regions. The two panels of Figure 11 show the CMD of the inner and outer regions, selected such that they have a similar total number of sources *in the bundles used for the SFH derivation* (∼2300). This occurs at $r = 1.38 r_h$. Interestingly, the overall morphology of the CMD does not change strongly as a function of radius. In the following we analyze in detail the differences in the SFH and how these reflect in the variation of the CMD morphology. The CDM of the outer regions, already presented in the right panel of Figure 3, clearly demonstrates that there is marginal evidence for the presence of And XVI stars beyond $5 r_h$ ($r_e = 5\farcm0$).

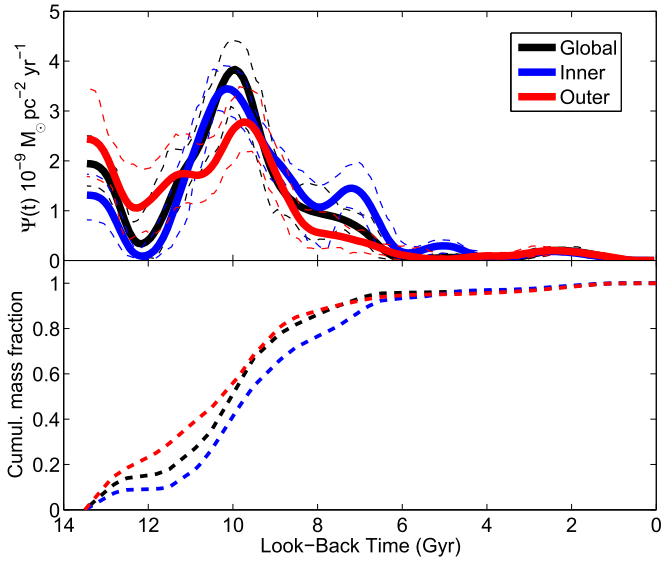

Figure 12. SFR derived for the inner and outer regions of And XVI. The star formation was slightly more prolonged in the inner than in the outer region, but no strong gradient was found.

6.1. The Spatially and Temporally Extended SFH of And XVI

To guide the eye, we overplotted on Figure 11 two isochrones from the BaSTI database, assuming $Z = 0.0003$ and ages = 6, 8 Gyr. Comparing the two panels, we found that the region between the two curves is slightly more populated in the inner (276 stars) than in the outer region (191 stars), suggesting that the SFR ∼6 Gyr ago was higher in the inner than in the outer region. It also may indicate that the star formation was slightly more prolonged toward the center of And XVI, as commonly found in nearby dwarf galaxies, though the effect looks small. It is remarkable that And XVI was able to sustain star formation for at least 6 Gyr over a vast fraction of its main body.

To support this finding, we derive the SFH in the two elliptical regions, in an identical way as for the full galaxy. The results are shown in Figure 12, where the calculated SFRs versus time are overplotted. The figure shows that the main features are consistent in the inner, outer, and the global solutions. The SFR in both the central and external regions presents an initial peak followed by a decreased activity. The main peak is recovered at similar age (∼10 Gyr ago), and star formation continues to 6 Gyr in both regions. However, at the most recent epochs, it presents stronger activity in the central part compared to the outskirts, with a secondary peak occurring ∼7 Gyr ago. It must be stressed that the uncertainties are large, mostly owing to the small number of stars used to derive both solutions, and therefore such detailed comparison should be treated cautiously. However, the fact that And XVI was able to sustain star formation for at least 6 Gyr over its entire body remains a solid result. This is significantly different from what was found in other dwarfs. For example, the spatial variation of the SFH in LGS 3 and Phoenix (Hidalgo et al. 2013) indicates the presence of a gradient in the age of the youngest populations, which are confined in the central regions only. Similar conclusions have been reached also in the case of the MW satellites Fornax and Carina (de Boer et al. 2013, 2014), which are dominated by intermediate-age populations in the center and by purely old populations in the outskirts.

7. DISCUSSION

Given its size and luminosity, And XVI is somewhat at the boundary between classical and faint dwarfs. Figure 13 shows the absolute M_V magnitude of Local Group dwarfs as a function of their size (half-light radius, r_h) and metallicity. The data are from the compilation paper by McConnachie (2012), and the plots partially replicate his Figures 6 and 12 (see also Clementini et al. 2012, their Figure 1). Different symbols indicate LG dwarf galaxies of different morphological types, as labeled. We updated here the position of And XVI, shown as a black diamond, using the luminosity from Martin et al. (2016, submitted). And XVI occupies the faint tail of the M31 satellites sequence, being ∼1 mag brighter than M31 dwarfs of similar size, such as And XI and And XX. With respect to previous estimates (Ibata et al. 2007), the absolute M_V magnitude increased by ∼1.7 mag, moving And XVI significantly closer to the faint dwarf region ($M_V = -7.5$ mag), but nonetheless it is still ∼2–3 mag brighter than Galactic faint dwarfs of similar size such as Leo V and Ursa Major II.

And XVI is thus a low-mass satellite of M31, located relatively far from both its host (∼279 kpc) and the MW (∼575 kpc). The most striking feature of its evolution is that it was able to sustain star formation for ∼7 Gyr and, as proven in the previous section, over most of its body, with only a small spatial gradient in the sense that the youngest star formation (6–8 Gyr ago) was stronger in the inner regions. This occurrence is an interesting and peculiar feature among LG dwarfs. In fact, broadly speaking, it is something intermediate between the two typical observed behaviors. Following the nomenclature introduced by Gallart et al. (2015), we identify that the majority of dSph galaxies are *fast* systems, i.e., they have formed stars for a short amount of time at the oldest epochs (e.g., Draco, Ursa Minor, Cetus, Tucana). On the other extreme, *slow* dwarf galaxies that present current or recent star formation are characterized by continuous activity from the oldest to youngest epochs (e.g., Leo A, Cole et al. 2007; Leo T, Clementini et al. 2012; Weisz et al. 2012; DDO210, Cole et al. 2014; the Fornax dSph, de Boer et al. 2012a; del Pino et al. 2013; the Magellanic Clouds, Smecker-Hane et al. 2002; Noël et al. 2009; Meschin et al. 2014). Within this scheme, the dominant old peak of star formation makes And XVI similar to a *fast* system, but nonetheless the extended activity is typical of *slow* galaxies, though the quenching occurred ∼6 Gyr ago. What mechanisms influenced the evolution of And XVI? What favored the extended star formation, and what caused its termination?

We derived that the mass formed in the surveyed area during the first 2 Gyr is of the order of $\approx 3 \times 10^4\ M_\odot$ (15% of the total mass). Therefore, And XVI would have properties comparable to a typical faint dwarf, if star formation had been truncated at a similar epoch. This suggests that, despite the similar stellar mass back then, And XVI was not strongly affected by reionitazion, which is thought to be the strongest mechanism shutting down star formation in low-mass MW satellites (Brown et al. 2014). On the other hand, the properties of the old population in And XVI are reminiscent of those of the old population in the low-mass dIrr isolated galaxies, Leo A and Leo T, at least in terms of integrated quantities. On the one hand, the mean SFR of Leo A between 13.5 and 11.5 Gyr ago

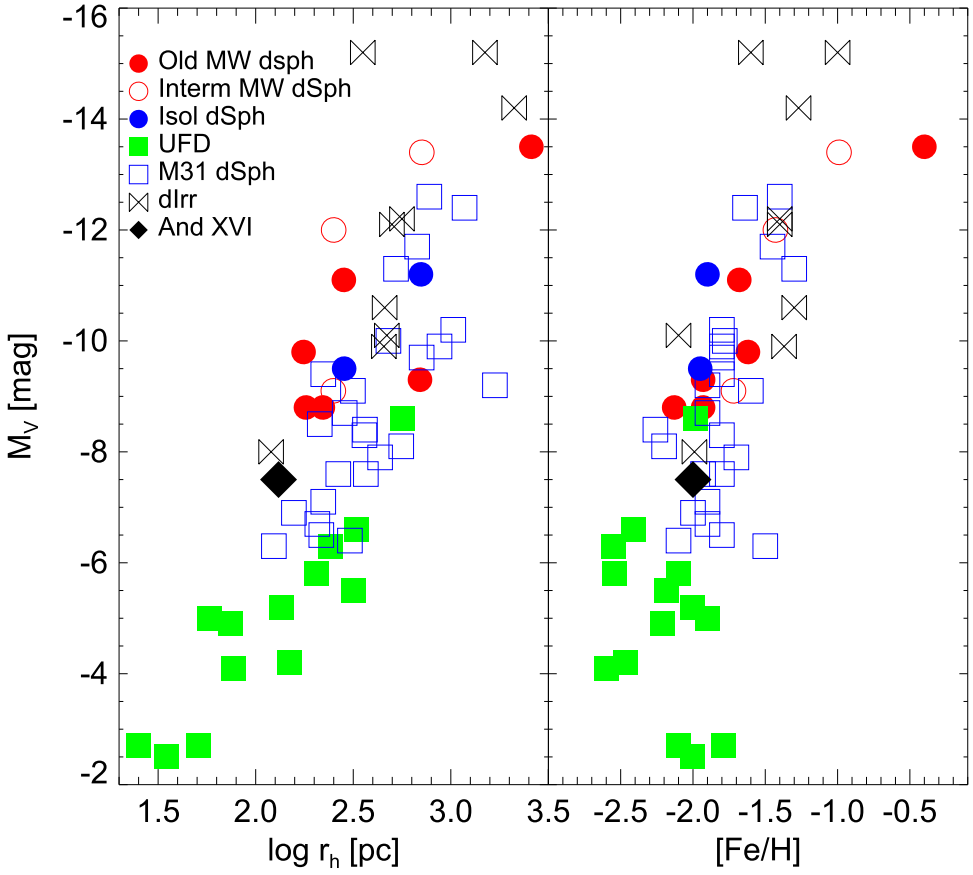

Figure 13. M_V magnitude vs. the logarithm of the half-light radius (left) and the metallicity (right) for LG dwarf galaxies of different morphological type. The data are from McConnachie (2012), but with updated values for And XVI. Different symbols indicate galaxies of different morphological types: red circle: MW dSphs (filled: purely old systems; open: systems with strong intermediate populations); blue circles: isolated dSphs (Cetus and Tucana); green squares: MW faint dwarf satellites; open squares: M31 dSph satellites; butterflies: dIrr systems (including transition types such as LGS3 and Phoenix).

was $\sim 2. \times 10^{-5}\,M_\odot\ \mathrm{yr}^{-1}$, implying that this dIrr formed in the first 2 Gyr a mass of stars of the order of $4 \times 10^4\,M_\odot$. This is within a factor of 2 of what was produced by And XVI.[20] Moreover, the number of RRL stars is very similar in both systems (8 versus 10; Bernard et al. 2013). On the other hand, Figure 13 also shows that, in both planes, And XVI is located remarkably close to Leo T, the lowest-mass star-forming galaxy known in the LG. In particular, And XVI is ~0.5 mag fainter than Leo T, which, despite its low mass (total mass $<10^7\,M_\odot$, Simon & Geha 2007; $M_\star \sim 1.2 \times 10^5\,M_\odot$, Ryan-Weber et al. 2008; thus comparable to that of And XVI), was able to form stars over a Hubble time (Clementini et al. 2012; Weisz et al. 2012).

This suggests that the initial properties of And XVI, Leo A, and Leo T were similar to those of a faint dwarf progenitor. Nonetheless, if the initial masses were similar, And XVI, Leo T, and Leo A would have been equally vulnerable as faint dwarfs to the quenching effect of reionization. This clearly does not seem to be the case, since in the SFH there is no trace of a strong damping effect during the early evolution, contrary to what occurs in faint dwarfs. *Possibly, this is indicating that the different evolution is dictated by the environmental conditions.* At present, Leo T is located in relative isolation quite similar to And XVI, at ~400 kpc from the MW and more than ~900 kpc from M31. Interestingly, the negative radial velocities of both Leo T and And XVI with respect to both spirals and the LG barycenter are compatible with them approaching the LG for the first time. Leo A is remarkably one of the most isolated systems at the fringes of the LG. Together with DDO210 and VV124, it belongs to the restricted group of dwarf galaxies that did not ever strongly interact with either the MW or M31 all along their history (McConnachie 2012). *The similarity of And XVI and these dIrrs may also indirectly support the idea that And XVI was initially located in a lower-density environment, far from both the ionizing radiation and the gravitational effect of the growing MW and M31, thus explaining the prolonged star formation despite the initial low mass. This has been proposed to be generally the case for* slow *systems (Gallart et al. 2015).*

Moreover, it has been suggested that And XVI is among the least dark matter dominated of the M31 satellites (Collins et al. 2014). This also might be an indication of a slower mass assembling history maybe related to the formation in a low-density environment. Although such small systems are expected to be strongly affected by reionization, the subsequent evolution may be driven by a complex interplay of mass assembly history, effect of the reionization, and effect of stellar feedback. Theoretical models by Benítez-Llambay et al. (2015) suggest that the stellar feedback acts as a regulator of the evolution of small galaxies after the reionization epoch: in those systems where the star formation started before the

[20] Taking into account the area covered by ACS data and the size of Leo A (Vansevičius et al. 2004), we estimate that this number might be underestimated by a factor of ≈2–3, thus not affecting the following discussion.

reionization, the stellar feedback contributes to sweep out the gas, causing a definitive termination in the star formation. In those systems where no stars formed before the reionization epoch, this contributes to heat up and disperse the gas, but is not strong enough to permanently remove the gas from these systems. This gas is later re-collected by the central halo and can start producing stars mostly at intermediate to young ages. Leo A, Leo T, and And XVI may fit in this scheme, and therefore they may be galaxies with mass below threshold for star formation before the reionization.

8. CONCLUSIONS

We have presented a detailed analysis of the And XVI dSph galaxy, satellite of M31, based on deep CMDs obtained from ACS data. The main conclusions can be summarized as follows:

1. We have derived three SFHs of And XVI using two different photometric reduction (DAOPHOT and DOLPHOT) and two stellar evolution libraries (BaSTI and Girardi), obtaining a very good agreement independently of the assumptions.
2. The SFH of And XVI at the oldest epochs seems different from both the MW and isolated dSphs, as the dominant peak occurred relatively late, around 10 Gyr ago, and is preceded by an initial peak at the oldest ages, followed by a period of decreased activity.
3. Despite the low stellar mass ($M \sim 10^5 M_\odot$), And XVI presents an extended star formation activity, which begun at the oldest epochs and was maintained until ~6 Gyr ago.
4. We detected nine variable stars, all RRL stars. Eight of them belong to And XVI, while one is compatible with being a more distant, M31 halo field star.
5. We provided a new estimate of the distance of And XVI, $(m - M)_0 = 23.72 \pm 0.09$ mag, based on the properties of RRL stars. We found that different methods (luminosity–metallicity relation, period–luminosity–metallicity relation) provide values slightly larger than previous estimates based on the RGB tip.
6. We discussed the properties of And XVI in comparison with other LG dwarfs. And XVI occupies the faint end of the dSph sequence. However, we found that if its star formation would have been truncated 12 Gyr ago, today it would closely resemble a faint dwarf galaxy in stellar mass.
7. The SFH of And XVI is consistent with a formation and early evolution in a low-density environment, which favored a slow mass assembly and prolonged star formation. A late arrival in the inner region of the LG may have been the cause of the termination in star formation occurring ~7 Gyr ago.

New data available for more M31 satellites, collected within the framework of this project, will allow us to build a fundamental sample to compare the MW, M31, and isolated dwarfs in the LG.

We are grateful to the anonymous referee for the pertinent comments that improved the paper. The authors thank M. Marconi and V. Braga for providing the coefficients of the period–luminosity relations. M.M. is grateful to G. Fiorentino and G. Bono for the discussion on the HB morphology and the RRL properties. Support for this work has been provided by the Education and Science Ministry of Spain (grants AYA2013-42781, AYA2014-56765-P). D.R.W. is supported by NASA through Hubble Fellowship grant HST-HF-51331.01 awarded by the Space Telescope Science Institute. M.B.K. is supported by the HST grants AR-12836 and AR-13888.

Facility: *HST* (ACS).

REFERENCES

Aparicio, A., & Gallart, C. 2004, AJ, 128, 1465
Aparicio, A., & Hidalgo, S. L. 2009, AJ, 138, 558
Bell, E. F., Slater, C. T., & Martin, N. F. 2011, ApJL, 742, L15
Benítez-Llambay, A., Navarro, J. F., Abadi, M. G., et al. 2015, MNRAS, 450, 4207
Bernard, E. J., Ferguson, A. M. N., Barker, M. K., et al. 2012, MNRAS, 420, 2625
Bernard, E. J., Monelli, M., Gallart, C., et al. 2009, ApJ, 699, 1742
Bernard, E. J., Monelli, M., Gallart, C., et al. 2010, ApJ, 712, 1259
Bernard, E. J., Monelli, M., Gallart, C., et al. 2013, MNRAS, 432, 3047
Bersier, D., & Wood, P. R. 2002, AJ, 123, 840
Bono, G., Caputo, F., Castellani, V., et al. 2003, MNRAS, 344, 1097
Brown, T. M., Tumlinson, J., Geha, M., et al. 2014, ApJ, 796, 91
Cacciari, C., Corwin, T. M., & Carney, B. W. 2005, AJ, 129, 267
Caputo, F., Marconi, M., Musella, I., & Santolamazza, P. 2000, A&A, 359, 1059
Castellani, V., & degl'Innocenti, V. 1995, A&A, 298, 827
Catelan, M. 2009, A&AS, 320, 261
Clementini, G., Cignoni, M., Contreras Ramos, R., et al. 2012, ApJ, 756, 108
Clementini, G., Gratton, R., Bragaglia, A., et al. 2003, AJ, 125, 1309
Cole, A. A., Skillman, E. D., Tolstoy, E., et al. 2007, ApJL, 659, L17
Cole, A. A., Weisz, D. R., Dolphin, A. E., et al. 2014, ApJ, 795, 54
Collins, M. L. M., Chapman, S. C., Rich, R. M., et al. 2014, ApJ, 783, 7
Collins, M. L. M., Martin, N. F., Rich, R. M., et al. 2015, ApJL, 799, L13
Conn, A. R., Ibata, R. A., Lewis, G. F., et al. 2012, ApJ, 758, 11
Coppola, G., Stetson, P. B., Marconi, M., et al. 2013, ApJ, 775, 6
Dall'Ora, M., Ripepi, V., Caputo, F., et al. 2003, AJ, 126, 197
de Boer, T. J. L., Tolstoy, E., Hill, V., et al. 2012a, A&A, 544, A73
de Boer, T. J. L., Tolstoy, E., Hill, V., et al. 2012b, A&A, 539, A103
de Boer, T. J. L., Tolstoy, E., Lemasle, B., et al. 2014, A&A, 572, A10
de Boer, T. J. L., Tolstoy, E., Saha, A., & Olszewski, E. W. 2013, A&A, 551, A103
de Jong, J. T. A., Harris, J., Coleman, M. G., et al. 2008, ApJ, 680, 1112
del Pino, A., Hidalgo, S. L., Aparicio, A., et al. 2013, MNRAS, 433, 1505
D'Onghia, E., Besla, G., Cox, T. J., & Hernquist, L. 2009, Natur, 460, 605
Fiorentino, G., Limongi, M., Caputo, F., & Marconi, M. 2006, A&A, 460, 155
Fiorentino, G., & Monelli, M. 2012, A&A, 540, A102
Gallart, C., Monelli, M., Mayer, L., et al. 2015, ApJL, 811, L18
Gallart, C., Zoccali, M., & Aparicio, A. 2005, ARA&A, 43, 387
Girardi, L., Bressan, A., Bertelli, G., & Chiosi, C. 2000, A&AS, 141, 371
Hidalgo, S. L., Aparicio, A., Skillman, E., et al. 2011, ApJ, 730, 14
Hidalgo, S. L., Monelli, M., Aparicio, A., et al. 2013, ApJ, 778, 103
Ibata, R., Martin, N. F., Irwin, M., et al. 2007, ApJ, 671, 1591
Ibata, R. A., Lewis, G. F., McConnachie, A. W., et al. 2014, ApJ, 780, 128
Irwin, M. J., Belokurov, V., Evans, N. W., et al. 2007, ApJL, 656, L13
Kaluzny, J., Kubiak, M., Szymanski, M., et al. 1995, A&AS, 112, 407
Kinemuchi, K., Harris, H. C., Smith, H. A., et al. 2008, AJ, 136, 1921
Koposov, S. E., Belokurov, V., Torrealba, G., & Wyn Evans, N. 2015, ApJ, 805, 130
Kroupa, P. 2002, Sci, 295, 82
Kunder, A., Stetson, P. B., Cassisi, S., et al. 2013, AJ, 146, 119
Lee, Y.-W. 1990, ApJ, 363, 159
Letarte, B., Chapman, S. C., Collins, M., et al. 2009, MNRAS, 400, 1472
Mac Low, M.-M., & Ferrara, A. 1999, ApJ, 513, 142
Madore, B. F., & Freedman, W. L. 1995, AJ, 109, 1645
Mapelli, M., Ripamonti, E., Battaglia, G., et al. 2009, MNRAS, 396, 1771
Mapelli, M., Ripamonti, E., Tolstoy, E., et al. 2007, MNRAS, 380, 1127
Martoni, M., Coppola, G., Bono, G., et al. 2015, ApJ, 808, 50
Martin, N. F., McConnachie, A. W., Irwin, M., et al. 2009, ApJ, 705, 758
Martin, N. F., Nidever, D. L., Besla, G., et al. 2015, arXiv
Martin, N. F., Schlafly, E. F., Slater, C. T., et al. 2013a, ApJL, 779, L10
Martin, N. F., Slater, C. T., Schlafly, E. F., et al. 2013b, ApJ, 772, 15

Martin, N. F., et al. 2016, ApJ, submitted
Mateo, M., Fischer, P., & Krzeminski, W. 1995, AJ, 110, 2166
Mayer, L., Governato, F., Colpi, M., et al. 2001, ApJL, 547, L123
Mayer, L., Mastropietro, C., Wadsley, J., Stadel, J., & Moore, B. 2006, MNRAS, 369, 1021
McConnachie, A. W. 2012, AJ, 144, 4
McConnachie, A. W., Irwin, M. J., Ibata, R. A., et al. 2009, Natur, 461, 66
Meschin, I., Gallart, C., Aparicio, A., et al. 2014, MNRAS, 438, 1067
Monelli, M., Cassisi, S., Bernard, E. J., et al. 2010a, ApJ, 718, 707
Monelli, M., Cassisi, S., Mapelli, M., et al. 2012, ApJ, 744, 157
Monelli, M., Gallart, C., Hidalgo, S. L., et al. 2010b, ApJ, 722, 1864
Monelli, M., Hidalgo, S. L., Stetson, P. B., et al. 2010c, ApJ, 720, 1225
Noël, N. E. D., Aparicio, A., Gallart, C., et al. 2009, ApJ, 705, 1260
Pietrinferni, A., Cassisi, S., Salaris, M., & Castelli, F. 2004, ApJ, 612, 168
Pietrinferni, A., Cassisi, S., Salaris, M., Percival, S., & Ferguson, J. W. 2009, ApJ, 697, 275
Richardson, J. C., Irwin, M. J., McConnachie, A. W., et al. 2011, ApJ, 732, 76
Ricotti, M., & Gnedin, N. Y. 2005, ApJ, 629, 259
Ryan-Weber, E. V., Begum, A., Oosterloo, T., et al. 2008, MNRAS, 384, 535
Salomon, J.-B., Ibata, R. A., Martin, N. F., & Famaey, B. 2015, MNRAS, 450, 1409
Santana, F. A., Muñoz, R. R., Geha, M., et al. 2013, ApJ, 774, 106
Schlafly, E. F., & Finkbeiner, D. P. 2011, ApJ, 737, 103
Simon, J. D., & Geha, M. 2007, ApJ, 670, 313
Skillman, E. D., Hidalgo, S. L., Weisz, D. R., et al. 2014, ApJ, 786, 44
Slater, C. T., Bell, E. F., & Martin, N. F. 2011, ApJL, 742, L14
Smecker-Hane, T. A., Cole, A. A., Gallagher, J. S., III, & Stetson, P. B. 2002, ApJ, 566, 239
Stetson, P. B. 1996, PASP, 108, 851
Susa, H., & Umemura, M. 2004, ApJL, 610, L5
The DES Collaboration, Bechtol, K., Drlica-Wagner, A., et al. 2015, ApJ, 807, 50
Tollerud, E. J., Beaton, R. L., Geha, M. C., et al. 2012, ApJ, 752, 45
Vansevičius, V., Arimoto, N., Hasegawa, T., et al. 2004, ApJL, 611, L93
Weisz, D. R., Skillman, E. D., Hidalgo, S. L., et al. 2014, ApJ, 789, 24
Weisz, D. R., Zucker, D. B., Dolphin, A. E., et al. 2012, ApJ, 748, 88
Willman, B., Masjedi, M., Hogg, D. W., et al. 2005, AJ, 129, 2692
Yang, S.-C., & Sarajedini, A. 2012, MNRAS, 419, 1362